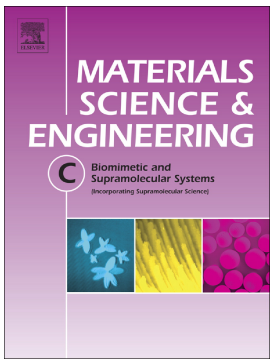

Low cost synthesis of reduced graphene oxide using biopolymer for influenza virus sensor

Shalik R. Joshi, Abhinav Sharma, Gun-Ho Kim, Jaesung Jang

PII: S0928-4931(19)33246-1

DOI: https://doi.org/10.1016/j.msec.2019.110465

Reference: MSC 110465

To appear in: *Materials Science & Engineering C*

Received date: 2 September 2019

Revised date: 1 November 2019

Accepted date: 17 November 2019

Please cite this article as: S.R. Joshi, A. Sharma, G.-H. Kim, et al., Low cost synthesis of reduced graphene oxide using biopolymer for influenza virus sensor, *Materials Science & Engineering C* (2019), https://doi.org/10.1016/j.msec.2019.110465

Low cost synthesis of reduced graphene oxide using biopolymer for influenza virus sensor

Shalik R. Joshi[1, ‡], Abhinav Sharma[2, ‡], Gun-Ho Kim[1, †], Jaesung Jang[1,3, †]

[1]Department of Mechanical Engineering, Ulsan National Institute of Science and Technology (UNIST), Ulsan 44919, Republic of Korea

[2]School of Materials Science and Engineering, UNIST, Ulsan 44919, Republic of Korea

[3]Department of Biomedical Engineering, UNIST, Ulsan 44919, Republic of Korea

[‡] these authors equally contributed to the work

Declarations of interest: None

KEYWORDS: bio-waste; thermal processing; 2D carbon; influenza virus; electrochemical biosensor

[†] Corresponding authors. Tel: +82-52-217-2323. E-mail: jjang@unist.ac.kr (Jaesung Jang)
Tel: +82-52-217-2413. E-mail: gunhokim@unist.ac.kr (Gun-Ho Kim)

ABSTRACT

A biocompatible, cost-effective, and scalable reduced graphene oxide (rGO) film was obtained from shellac using thermal treatment and its structural, chemical, and electrical properties were investigated. This thermally-decomposed rGO (TrGO) film exhibited good crystallinity, low sheet resistance, and high carbon content. TrGO flakes obtained from the film were dispersed and drop cast onto indium tin oxide/glass electrodes to fabricate label-free electrochemical immunosensors for the quantitative detection of the influenza virus H1N1 via electrochemical impedance spectroscopy.

These sensors exhibited high stability and reproducibility, both possibly ascribable to the high adhesion of TrGO due to its phenolic-OH moiety; the limits of detection were 26 and 33 plaque-forming units, respectively, in phosphate-buffered saline and diluted saliva. These cost-effective TrGO-based sensors showed great potential as reliable and robust nanomaterial-based biosensors for widespread clinical applications.

1. Introduction

Influenza is a significant threat worldwide [1-3]; among its three types (A, B, and C), influenza A virus can infect various warm-blooded animals, including birds, swine, humans, and other mammals [4]. In particular, the H1N1 subtype is currently the main cause of epidemics and pandemics, causing serious socio-economic losses worldwide [5, 6]. Various biosensors including quartz crystal microbalances [7, 8], interferometry [9], imaging ellipsometry [10], surface plasmon resonance [11] and ELISA test [12] have been developed for the detection of influenza virus. The application of the most common virus detection methods, such as the enzyme-linked immunosorbent assay, the nucleic acid-based assay via a polymerase chain reaction, and viral isolation and growth techniques, is limited by the multistep processing of samples, long diagnostic times, high costs, and trained personnel. On the contrary, electrochemical detection methods usually present several advantages such as simple instrumentation, compatibility with miniaturized and portable systems, fast response time [13], and ability to perform quantitative analysis with low detection limit [14, 15].

Various nanomaterials have been incorporated into electrochemical sensors for the detection of different biomolecules [16-18] to enhance their sensitivity. In particular, the large surface area, high charge carrier mobility, and high electrical conductivity [19-22] make reduced graphene oxide (rGO) an excellent electrochemical biosensor material. A common rGO synthesis pathway relies on the chemical oxidation of high-quality graphite to produce soluble graphene oxide (GO) which

undergoes chemical reduction to yield desirable electrical properties. Although this chemical approach is suitable for the large-scale and inexpensive production of thin rGO sheets [23, 24], its oxidation and reduction steps require toxic reagents, leading to a significant amount of structural disorder or defect, which reduces its electrical conductivity and the sensitivity of the sensors [25].

Shellac, an inexpensive (<2 USD/kg) natural biopolymer secreted by a female lac bug, has excellent biocompatibility, as recently shown in biomedical organic devices [26]. It consists of a long aliphatic carbon chain which facilitates cyclization at a much lower temperature than that for synthetic polymers [27] such as polystyrene and poly (methyl methacrylate) and, thereby, can allow the formation of high-quality graphene-like sheets without any chemical reduction process. Few studies have introduced a single-step synthesis of rGOs from shellac by thermal annealing (900 ˚C in an inert atmosphere), achieving excellent corrosion resistance, giant magnetoresistance, and antimicrobial properties [28-30]. However, to the best of our knowledge, the bio-sensing capability of rGO films synthesized from shellac has not been demonstrated, yet.

Here, we propose the fabrication of a label-free electrochemical biosensor by using rGO films obtained from shellac for detecting the influenza virus H1N1. Shellac was subjected to a simple thermal treatment to produce high quality reduced graphene oxide (TrGO) films at 700 ˚C, which is lower than that of the previous thermal decomposition processes. The resultant films were characterized by X-ray diffraction (XRD), X-ray photoelectron spectroscopy (XPS), Raman spectroscopy, Fourier transform infrared (FTIR) spectroscopy, and four-point probe measurements, suggesting the presence of high-quality rGO, and several characteristics of the fabricated sensors such as sensitivity, selectivity, limit of detection, and reproducibility were also assessed.

2. Experiments

2.1 Materials

The following materials were used: shellac flakes (PH-541-332-8003; Shellac Shack, USA); ethanolamine (≥98%, E9508; Sigma-Aldrich, USA); dimethylformamide (DMF) (D1021; Biosesang, Republic of Korea); PBSE (P130; Thermo Scientific, USA); PBS (pH 7.4, 10×; Life Technologies, Republic of Korea); glass wafers (6 inches, Pyrex 7740; iNexus, Inc., Republic of Korea); H1N1 antibodies (AB1074; Merck Millipore, USA); MS2 bacteriophage (ATCC® 15597-B1™; Koram Biogen Corp., Republic of Korea). Influenza B virus (KBPV-VR-34), influenza A virus H1N1 (KBPV-VR-76), and adenovirus (KBPV-VR-4) were obtained from the South Korean Bank of Pathogenic Viruses. Deionized (DI) water (18.2 MΩ) prepared using the Millipore water purification system was used for all the experiments.

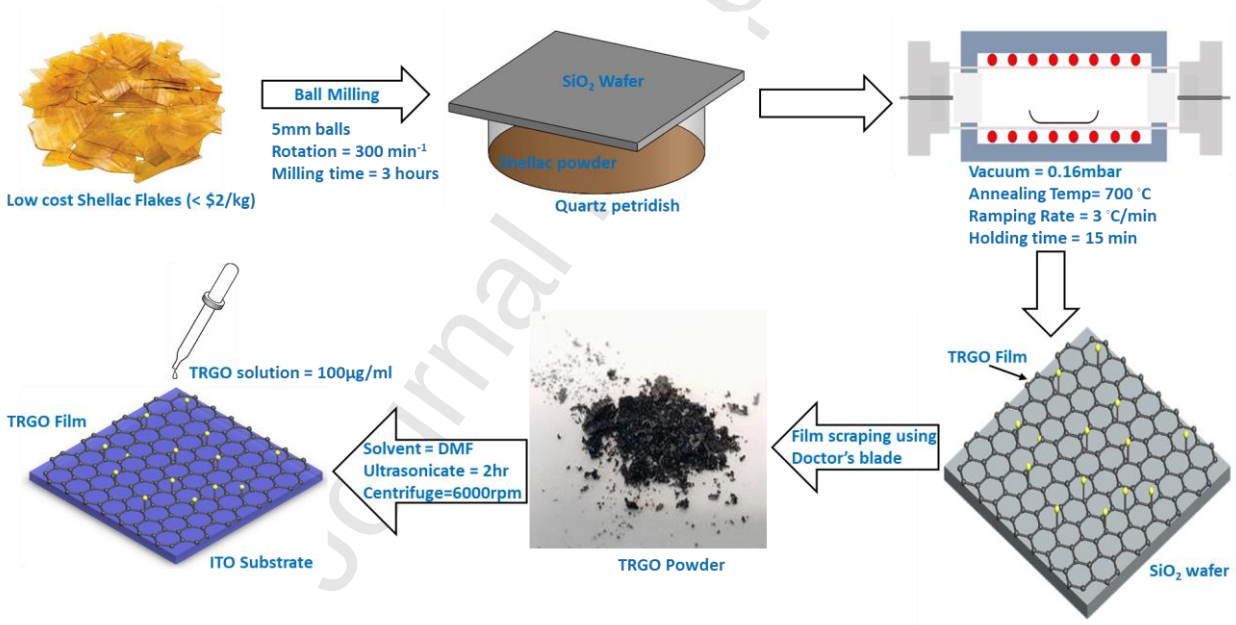

Scheme 1: Schematic illustration to display the synthesis route of TrGO using Shellac biopolymer.

2.2. Synthesis of homogenous TrGO solution

The shellac flakes were crushed into fine powders and put in a quartz petri dish, which was covered with a silicon wafer coated with a 100 nm thick silicon dioxide layer. This petri dish was

placed in a vacuum (0.06 mbar) furnace for thermal decomposition. The temperature was increased to 700 °C with a ramping rate of 3 °C/min and holding time for 15 min, to deposit a TrGO film on the wafer. The TrGO film was scraped off using a blade to obtain free-standing TrGO flakes. The resulting flakes (2 mg) were dispersed into DMF (2 mL) by ultrasonication for 1 h to form a stable solution, which was diluted with additional DMF to prepare a homogeneous solution (10 µg/ml) through further ultra-sonication for 1 h, followed by centrifugation at 6000 rpm for 30 min. The supernatant was collected for the experiments, as shown in Scheme 1.

2.3. Bio-functionalization of the TrGO/ITO/glass electrodes

A glass wafer was cleaned with a piranha solution (H_2SO_4: H_2O_2 = 3:1) for 10 min followed by rinsing with DI water and drying with N_2 gas. An ITO layer (100 nm) was deposited on the wafer by radiofrequency sputtering and successively annealed at 400 °C for 1h. The as-coated wafer was diced into strips (1.5 cm × 0.5 cm) and were sequentially cleaned in acetone, methanol, and DI water and, then, dried with N_2 gas, to be used as working electrodes. The resulting ITO/glass electrodes were immersed into a solution consisting of H_2O, NH_4OH, and H_2O_2 (5:1:1 (v/v)) in an oven at 60 °C for 30 min for hydrolysis and the solution was then quickly quenched with DI water for 2 min. Next, these electrodes were thoroughly flushed with DI water several times and dried with N_2 gas. After hydrolysis, the wetting properties of the ITO surface is changed, which played a pivotal role in obtaining highly continuous and homogeneous TrGO films on the ITO/glass substrate. Furthermore, the presence of phenolic (-OH) groups in TrGO enabled the formation of covalent bonds at the interface.

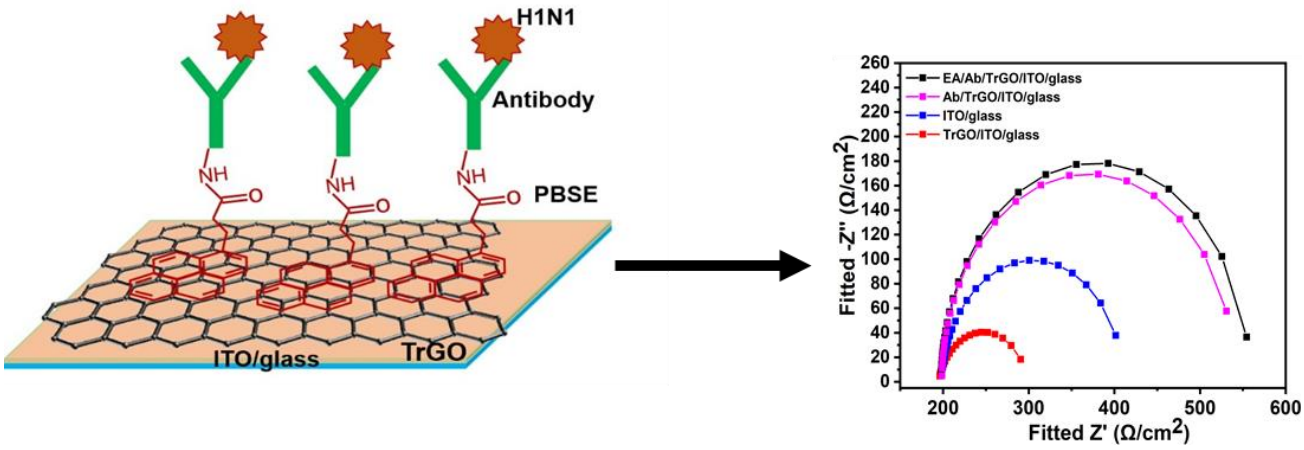

Scheme 2: Schematic of the proposed thermally-decomposed reduced graphene oxide (TrGO)-based immunosensor for the detection of the influenza virus H1N1. The electrochemical impedance spectroscopy was used in the study as the final signal for the detection of influenza H1N1 viruses.

The previously collected TrGO suspension (5 µL) dropped cast onto these cleaned strips and dried at 60 °C for 1 h; after the formation of a homogeneous TrGO film, the electrodes were washed with DI water and dried with N_2 gas. The resulting TrGO/ITO/glass electrodes were functionalized with 5 mM PBSE (linker) in DMF at room temperature for 1 h and, then, treated with DMF and DI water. PBSE makes stable noncovalent interactions via π-electron-donating and accepting and offers covalent attachment of biomolecules through their amine groups. The electrodes were incubated with H1N1 antibodies (20 µg/mL) in 1× PBS at 37 °C for 2 h, washed with 1× PBS, and air-dried at room temperature. Then, the Ab/TrGO/ITO/glass electrodes were incubated with 100 mM ethanolamine (EA), a blocking buffer, at room temperature for 30 min to prevent non-specific binding and, successively, washed with 1× PBS. The electrochemical measurements were performed on the target influenza virus (10–10000 PFU/mL) in 1× PBS and 80% saliva (v/v)–1× PBS solutions (Scheme 2).

2.4. Characterization

The XRD measurements were performed on a Bruker D8 Advance diffractometer with Cu Kα radiation (30 KV, 30 mA), a diffracted beam monochromator, and a step-scan mode with a step of 0.04° (2θ) and 4 s per step. The Raman spectra of the TrGO flakes were measured in a back-scattering geometry by using an ultra-high throughput spectrometer (WiTec alpha300r, λ = 632nm). The XPS measurements were conducted with a K-alpha XPS system (Thermo Fisher Scientific, UK) equipped with a double-focusing hemispherical analyzer and a monochromatic Al Kα source (1486.6 eV); the spectra were acquired in the constant analyzer energy mode for narrow regions, with a pass energy of 25 eV. The sample charging was compensated with the system flood gun having low-energy electrons. The vacuum of the main chamber was maintained at 1×10^{-9} mbar during the entire process. The Thermo Scientific Avantage software was used for digital acquisition and data processing; the spectral calibration was performed by using the automated calibration routine and the internal Au, Ag, and Cu standards supplied with the XPS system. The FTIR spectra were collected using an FTIR spectrometer (model 670, Agilent, USA) with pure KBr as the background. The surface resistance of the TrGO films was measured with a four-point probe system (CMT-2000N, Advanced Instrument Technology). The thickness of the film was measured using atomic force microscopy (Multimode V, Bruker, USA) in tapping mode. The morphological studies were conducted using an HRTEM microscope (JEM-2100F); for this analysis, well-suspended TrGO was prepared and drop cast onto a copper TEM grid.

The TrGO/ITO/glass electrodes with surface functionalization were characterized via cyclic voltammetry (CV), differential pulse voltammetry (DPV), and electrochemical impedance spectroscopy (EIS) measurements in PBS containing 5 mM $[Fe(CN)_6]^{3-/4-}$ and 0.5 M KCl. All the electrochemical data were recorded with the working electrode (ITO/glass, 0.2 cm × 0.5 cm), the reference electrode (Ag/AgCl), and the counter electrode (Pt) by using an Autolab System

(PGSTAT204, Metrohm, Netherlands) controlled by the NOVA 1.10 software. Two biosafety level 2 (BSL2) cabinets were used in this study for handling the influenza viruses.

3. Results and discussion

3.1. Analytical characterization of TrGO

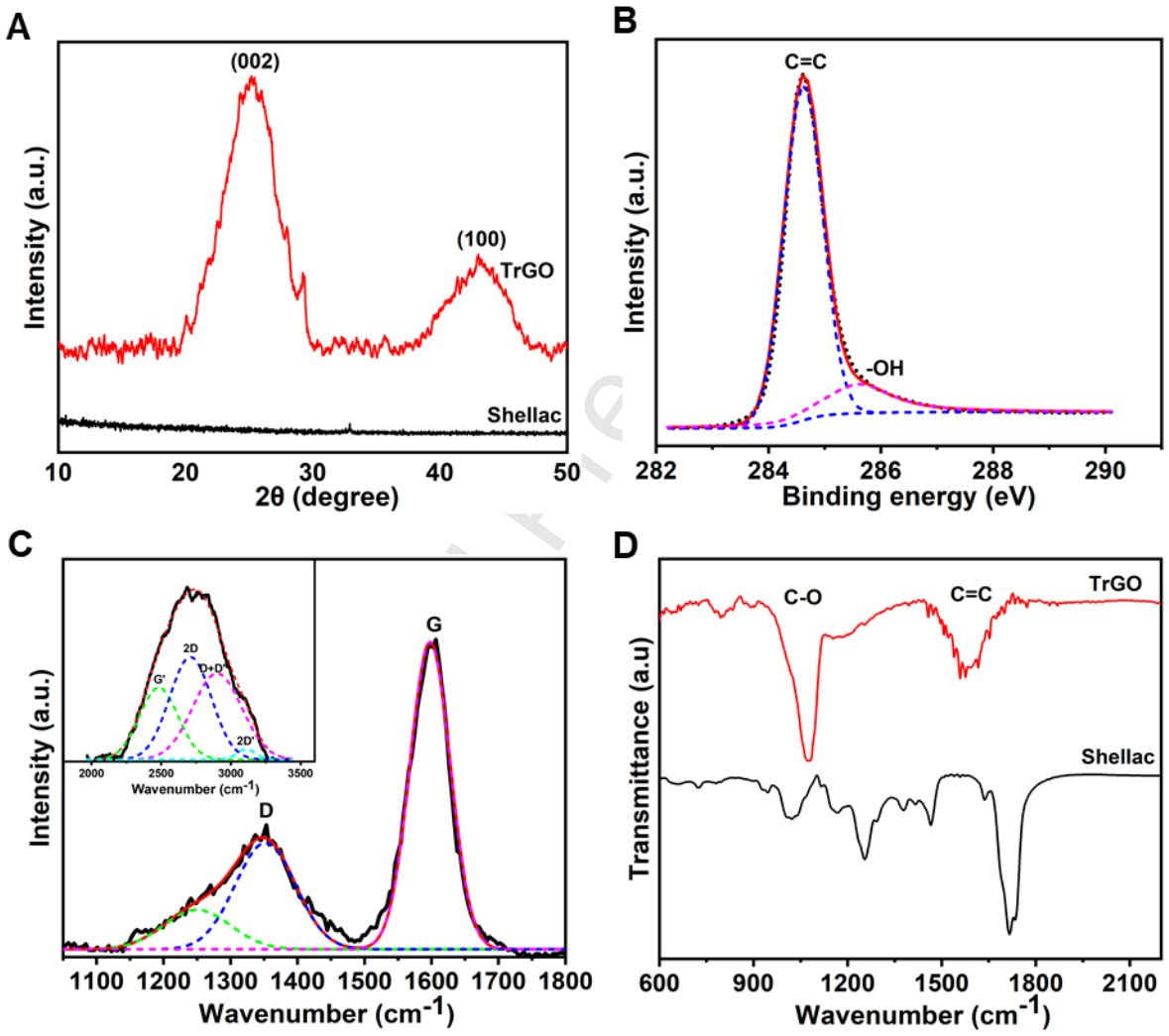

Fig 1. Characteristics of the thermally-decomposed reduced graphene oxide (TrGO) films synthesized from shellac: (a) X-ray diffraction spectra revealing its crystalline nature; (b) high-resolution C 1s X-ray photoelectron spectra; (c) Raman spectra showing the G and D bands along with (inset) the 2D band; (d) Fourier transform infrared (FTIR) spectra showing its highly graphitic

nature.

XRD spectra were taken for both shellac and the synthesized TrGO films to evaluate their bulk structural properties (Figure 1a). The absence of peaks in the case of shellac, like for other synthetic polymers, confirmed its amorphous nature, whereas the TrGO films exhibited a diffraction peak at 25.2° ((002) plane), indicating that it comprised largely free nanosheets [8]; regarding this peak, we estimated an interlayer spacing of 0.35 nm via the Bragg equation and its full width half maximum was smaller than the values reported [31] for conventional rGO, suggesting that the synthesized TrGO consisted of well-ordered two-dimensional sheets. Another peak at 42.5° was also observed in the TrGO spectrum, probably due to incomplete oxidation.

The transmission electron microscopy (TEM) images of TrGO revealed slightly transparent sheets with multiple layers overlapped with each other, as shown in Figure 2a. Furthermore, the high resolution (HRTEM) micrographs showed (Figure 2b) that the samples contained few-layer thick crystalline nanosheets. The observed average lattice spacing of ~0.34 nm, as shown in Figure 2c, corresponds to the distance between two neighboring (002) planes in graphitic materials, confirming the XRD results. The fast Fourier transform pattern (Figure 2d) revealed a hexagonal crystal pattern quite similar to that observed for graphene in previous studies [28, 29]. The topography and the thickness of the TrGO films have been investigated using atomic force microscopy, in tapping mode and the results are displayed in Figure S3. The results display a few TrGO sheets with a size of more than 3µm. The average thickness of the sheet was estimated to be around 18nm, which is slightly larger than what has been observed using HRTEM (~15nm). The surface also displays a lot of wrinkles and partially folded edges on the surface of TrGO nanosheets due to its high surface tension [32].

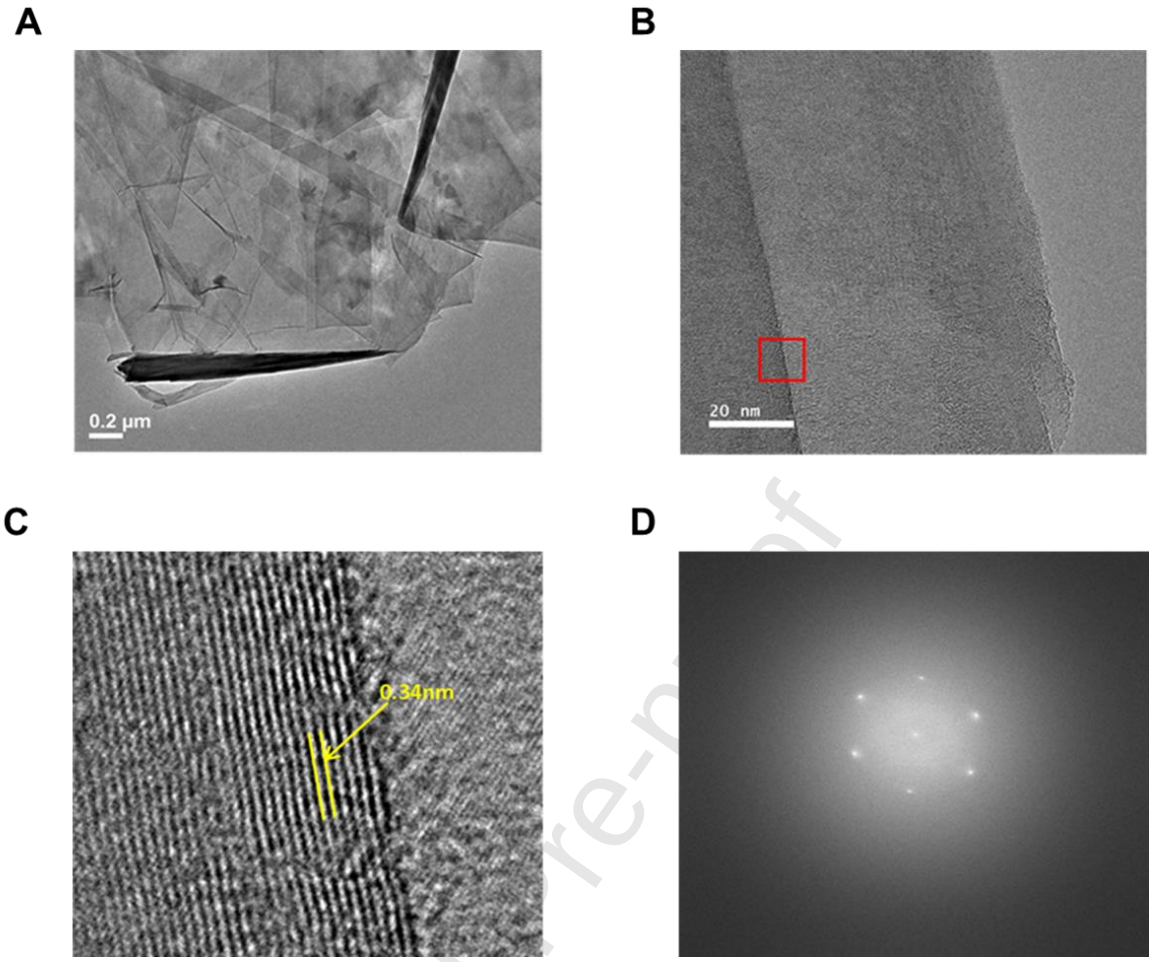

Figure 2. Microcrystalline structural analysis of thermally reduced graphene oxide| (a) Transmission electron microscope images of few-layered thermally-decomposed reduced graphene oxide (TrGO) obtained from shellac. (b) High-resolution TEM (HRTEM) image taken at the edge of the TrGO flake showing few-layered features. (c) Zoomed-in image of HRTEM (square box) showing the crystalline nature of TrGO. (d) Selective area diffraction pattern of TrGO showing the hexagonal structure of TrGO.

X-ray photoemission spectroscopy was used to identify the chemical structure and elemental composition. Figure S1 shows the XPS survey spectrum of Shellac and TRGO film processed at 700 °C. The survey spectrum clearly shows the presence of carbon and oxygen, as the main constituents of the biopolymer. It can be clearly seen that, after thermal reduction, the intensity of oxygen has

been reduced dramatically. The atomic weight percentage for carbon and oxygen, for Shellac, was 60% and 40%, respectively. However, for TRGO film treated at 700 °C, carbon content has been increased to 97% whereas the oxygen content has been dramatically reduced to 3%. This high carbon/oxygen ratio is favorable to electrical conductivity and much higher than in conventionally derived rGO-based materials (e.g., hydrazine-reduced GO has a ~5% oxygen content [25]) (Table S1). Figure 1b shows the high-resolution C-1s spectra of shellac and after heat treatment at 700 °C. The shellac peak is deconvoluted into three main features at 284.8eV, 286.4 eV and 288.1 eV which can be assigned to C-C, C-OH and -COOH functional groups, respectively. However, after thermal reduction at 700 °C, the feature at 284.8 eV shifts towards low binding energy, i.e. at 284.4 eV, confirms the transition of sp^3 to sp^2 hybridized carbon networks [33]. At this reduction temperature, the TrGO exhibits a similar XPS spectrum to that of natural graphite, dominated by C=C bonds with a small tail at high binding energy. This reveals a significant loss of several oxygen functional groups during the thermal treatment, results in better graphitization.

Given the small difference in the binding energy between sp^2 and sp^3 bonded carbon atoms in the C 1s peak, the Raman spectra were also acquired to obtain more detailed information on the sp^2 ones (Figure 1c). The Raman spectra for shellac displays a broad hump, as shown in Figure S2, suggests that vibration modes of shellac are Raman inactive. However, for TrGO, the D (~1352 cm^{-1}) and G (~1598 cm^{-1}) peaks observed were due to, respectively, the in-plane breathing mode of the A_{1g} symmetry, assigned to the structural disorder [34], and the E_{2g} phonons of the sp^2-hybridized carbon atoms [34]. The small peak at ~1250 cm^{-1} was attributed to the presence of hydroxyl groups [35], also shown in the XPS data (Figure 1b). The 2D band is usually associated to the number of layers of graphene sheets and their relative orientations [36, 37]; the inset in Figure 1c shows a broad 2D peak that was deconvoluted into four peaks and might be due to the random orientation of different planes of the TrGO nanosheets [37]. The estimated intensity ratios of the D and G peaks (I_D/I_G) and the G

and 2D ones (I_{2D}/I_G) were 36% and 19%, respectively, demonstrating the low defect concentration and superior graphitization of the current TrGO than those for GO and rGO to previous reports [38] (Table S1).

FTIR spectroscopy was performed to investigate the evolution of the functional groups during the thermal treatment of shellac (Figure 1d). The FTIR spectrum of shellac was consistent with previous studies [39, 40], while that of TrGO clearly showed the elimination of most oxygen-containing groups. The peak at ~1075 cm^{-1} was attributed to the C–O stretching vibrations, whereas that at ~1590 cm^{-1} was assigned to the C=C skeletal vibrations of the graphitic domains, similarly to conventional rGO [41]. The FTIR results well agreed with the XPS, Raman, and XRD data, confirming that the oxygen functional groups of shellac were effectively eliminated (except the phenolic OH groups) during the thermal treatment, which resulted in high-quality TrGO flakes.

Sheet resistance (R_s) is an indicator of the structural integrity of the long-range π-conjugation. Shellac, an insulating polymer with R_s > 100 MΩ/sq (instrument limit), contains long aliphatic chains along with with cyclic five- and six-membered carbon rings attached to several oxygen functional groups. As the temperature increased up to 700 °C, these carbon units began to dissociate into carbon atoms to form sp^2-hybridized carbon networks [42]; such sp^2-hybridized carbon chains are susceptible to cyclization, which leads to graphitization. The decomposition of shellac at a lower temperature compared to other synthetic polymers can be attributed to these long aliphatic chains [27]. In the synthesized TrGO, R_s was reduced to ~200 Ω/sq, which is the smallest value achieved in solution-processed rGO to date [25]. This result is consistent with the highest degrees of de-oxygenation and graphitization, as shown earlier in this study. Inspired by all these superior properties revealed by the proposed TrGO (Table S1), we fabricated a label-free electrochemical sensor for detecting the influenza virus H1N1.

3.2. Electrochemical characteristics of TrGO/indium tin oxide (ITO)/glass electrodes

Figure 3a shows the cyclic voltammograms (CVs) of the following electrodes: ITO/glass, GO/ITO/glass, hydrazine-treated rGO/ITO/glass, and TrGO/ITO/glass. The peak current of the GO/ITO/glass electrode (98.77 μA), where the GO was synthesized via the modified Hummers method, was lower than that of the bare ITO/glass one (158.71 μA) due to the electron transfer blocking by GO. In the TrGO/ITO/glass electrode, it increased up to 251.18 μA, above the values for both the hydrazine-treated rGO/ITO/glass (219.67 μA) and GO/ITO/glass ones; such a large peak current can be ascribed to the high conductivity, large surface area, and unique electron transfer property of TrGO, which could further enhance the redox conversion. DPV and EIS were also performed and the results well agreed with the CV data (Figure S4 and Figure 3b). The higher peak current of the TrGO/ITO/glass electrode also indicates that the proposed TrGO was highly conductive compared to both GO and hydrazine-treated rGO. The charge transfer resistance (R_{ct}) for the ITO/glass and rGO/ITO/glass electrodes was 220 and 138.92 Ω respectively, but only 98.7 Ω for the TrGO/ITO/glass one, further confirming this highly conductive nature.

Figure 3c shows the CVs of ITO/glass electrodes with and without successive functionalization (TrGO/ITO/glass, antibody (Ab)/TrGO/ITO/glass, and ethanolamine (EA)/Ab/TrGO/ITO/glass). The peak current increased after the TrGO deposition due to its high electron transfer characteristics and decreased down to 142.7 μA after the immobilization of the H1N1 antibodies via 1-pyrenebutanoic acid succinimidyl ester (PBSE) linker because of their insulating behavior. It decreased down to 138.2 μA after EA immobilization, further blocking the electron transfer. Moreover, the DPV and EIS results exhibited the same trends as the CV data (Figure S5a and Figure 3d).

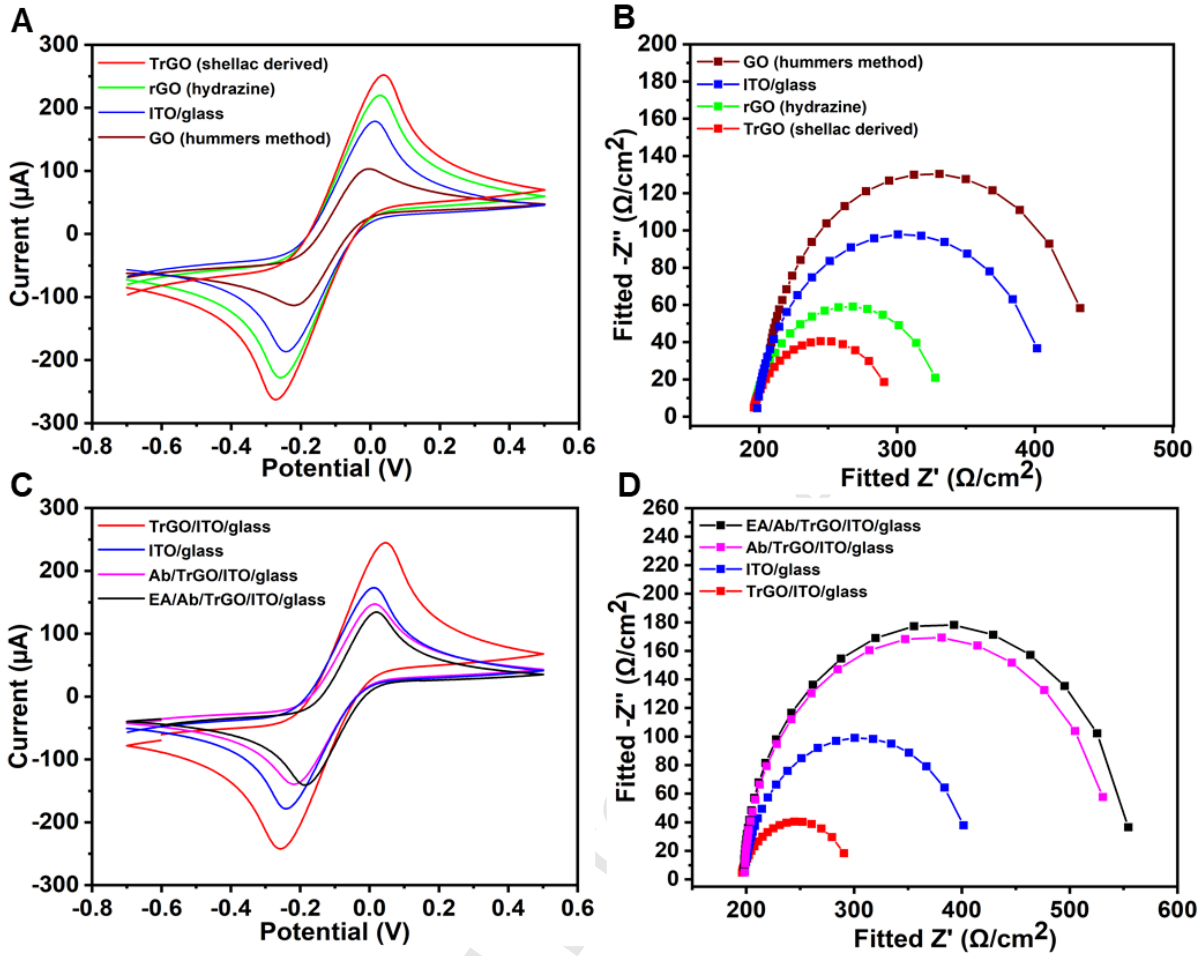

Figure 3. Electrochemical properties of thermally reduced graphene oxide| (a) Cyclic voltammograms (CVs) at a scan rate of 50 mV/s, and (b) Nyquist plots of indium tin oxide (ITO)/glass, graphene oxide (GO)/ITO/glass, hydrazine-treated reduced GO (rGO)/ITO/glass, and thermally-decomposed rGO (TrGO)/ITO/glass electrodes in the presence of 1× phosphate-buffered saline (PBS) solution containing 5 mM $[Fe(CN)_6]^{3-/4-}$ and 0.5 M KCl as redox mediator. (c) CVs and (d) EIS (Nyquist plots) of ITO/glass, TrGO/ITO/glass, antibody (Ab)/TrGO/ITO/glass, and ethanolamine (EA)/Ab/TrGO/ITO/glass in the presence of 1× PBS containing 5 mM $[Fe(CN)_6]^{3-/4-}$ and 0.5 M KCl as redox mediator.

The optimal concentrations of TrGO suspension (1 µg/mL to 500 µg/mL) and H1N1 antibody (1 µg/mL to 50 µg/mL) were also estimated using DPV (Figure 4). During the optimization for the

TrGO concentration (Figure 4a), the current increased with increasing concentration and reached a maximum at 100 µg/mL. However, a further increase in the concentration of TrGO showed a decrease in current, which motivated us to use 100 µg/mL as the optimum concentration during the entire experiment. Furthermore, for the optimal H1NI antibody concentration (Figure 4b), a maximum decrease in the current was observed at an antibody concentration of 20 µg/mL, following which saturation was observed. Thus, we used 20 µg/mL as the optimum condition, and sufficient change in current showed the efficient attachment of antibody on the TrGO surface. The scan rate effects on the EA/Ab/TrGO/ITO/glass electrode are shown in Figure S6.

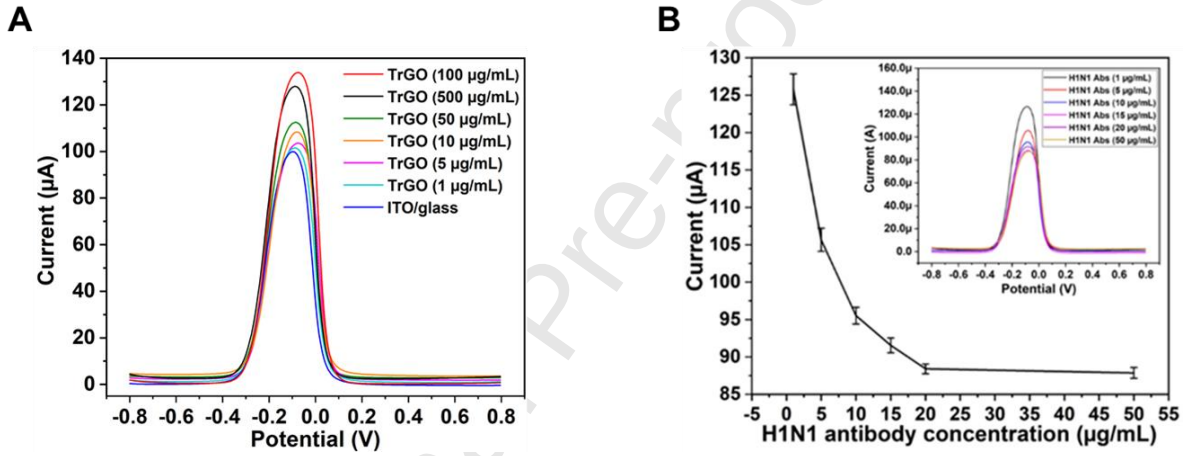

Figure 4. Optimization of TrGO and H1N1 antibody concentrations| (a) Optimization of TrGO concentration (1 µg/mL to 500 µg/mL) on ITO/glass electrodes. **(b)** The changes in current with H1N1 antibody concentrations (1 µg/mL to 50 µg/mL) on the TrGO/ITO/glass electrodes (the inset showing DPV response) in the presence of 1× PBS containing 5 mM $[Fe(CN)_6]^{3-/4-}$ and 0.5 M KCl as redox mediator. The error bars represent the standard deviations based on four independent measurements.

3.3. Electrochemical detection of the influenza virus H1N1

Standard sample solutions (10–10000 PFU/mL) were prepared from a stock solution of influenza virus H1N1 in 1× phosphate-buffered saline (PBS) and saliva samples. Fresh saliva was obtained after rinsing of the mouth with drinking water and hold saliva in the mouth without or minimize swallowing, and collected into Eppendorf tube, followed by centrifugation at 12000 rpm for 10 min. The upper part of the saliva sample was collected carefully and make dilution 80% (v/v) with the working buffer (1× PBS) to prepare various concentrations influenza virus (10–10000 PFU/mL) prior to electrochemical measurements.

To evaluate the selectivity of the sensors, influenza B virus, adenovirus, and MS2 bacteriophage were also prepared likewise. The virus concentrations in both 1× PBS and saliva samples were measured via EIS in the 0.1–100 kHz frequency range at a potential of 0.1 V and an amplitude of 10 mV. At this optimized potential (0.1V), we observed the information about the charge transfer reaction and diffusion process, and able to calculate the Charge transfer resistance (Rct) from the diameter of the semicircle and diffusion coefficient as well.

The resulting R_{ct} calibration curves are shown in Figure 5 along with the Nyquist plots of the immunosensors, where the diameters of the semi-circles represent the R_{ct} values; the R_{ct} increased with the virus concentration in both the sample types. The electrochemical immunosensors exhibited linearity (R^2 = 0.95 and 0.90 for the 1× PBS and saliva samples, respectively) with respect to the logarithm of the virus concentrations. According to the abovementioned calibration curves and a signal-to-noise ratio of 3, the detection limits determined for the H1N1 subtype in 1× PBS and the saliva samples were 26 and 33 PFU/mL, respectively. Since the concentration of the influenza viruses in saliva and nasal samples usually ranges between 10^3 and 10^5 $TCID_{50}$/mL, the proposed TrGO-based electrochemical sensor can be considered sufficiently sensitive for clinical applications [43]. A detailed comparison with previously reported biosensors is also shown in Table 1.

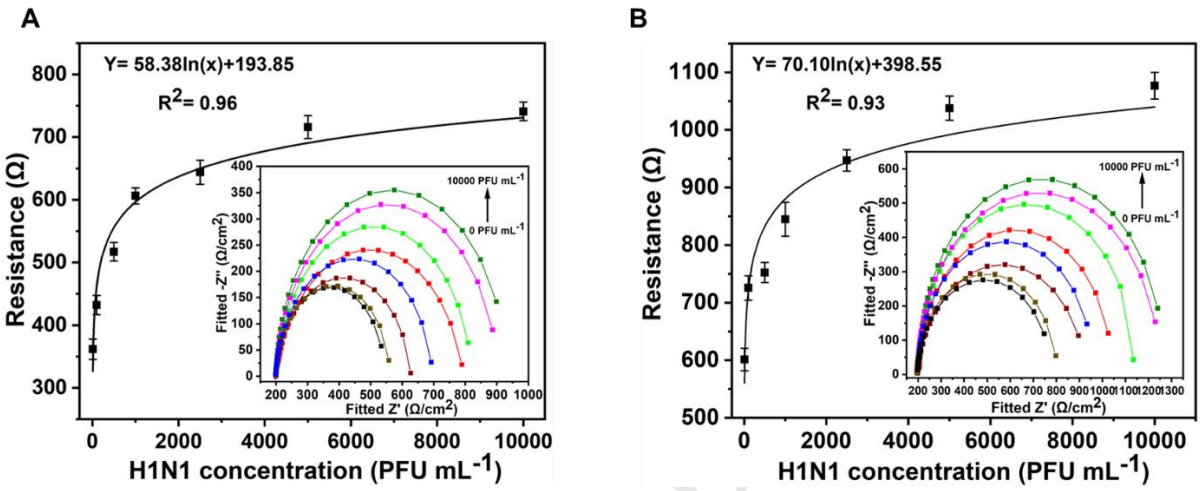

Figure 5. Responses to the TrGO-based biosensors with logarithmic fits. Calibration curves based on electrochemical impedance spectra for the quantitative detection of H1N1 virus concentrations between 0 and 10000 (10, 100, 500 1000, 2500, 5000, and 10000) plaque-forming units/mL in (a) phosphate-buffered saline (PBS, pH 7.4, 1×) and (b) spiked saliva samples in PBS. The insets show the Nyquist plots in the presence of 1× PBS containing 5 mM $[Fe(CN)_6]^{3-/4-}$ and 0.5 M KCl as a redox mediator. The error bars represent the standard deviations based on four independent measurements.

Table 1. Comparison table of electrochemical immunosensors for the detection of influenza A viruses. Ab: antibody, Au: gold, BDD: boron-doped diamond, CA: chronoamperometric, CA: cystamine, CPE: carbon paste electrode, DPV: differential pulse voltammetry, EIS: electrochemical impedance spectroscopy, GCE: glassy carbon electrode, GO: graphene oxide, MB: methylene blue,

Sensor type	Substrate	Bio receptors	Antigen	Detection	References

PEDOT-OH: poly(3,4- ethylene dioxythiophene), PFU: plaque-forming units, RGO: reduced graphene oxide, Si: silicon, SPCE/PVC: screen-printed carbon electrode/polyvinylchloride membrane, TsO/TOPAS: tosylate.

				limit	
Amperometric	SPCE/PVC membrane	(4,7di-OMe)Sa2,3Gal or (4,7di-OMe)Sa2,6Gal	Influenza virus	100 PFU/mL	[1]
EIS	PEDOT-OH:TsO electrode/TOPAS polymer	Aptamer	H1N1	10 PFU/mL	[2]
EIS	Au electrode	Anti-H5N1 antibody	H5N1	0.7×10^{3} PFU/mL	[44]
EIS	Au electrode	Anti-M1 ab/colloidal gold particles/Au electrode	M1 protein of H1N1 virus	80-100 virions/µL or 20 pg/mL	[15]
EIS	BDD electrode/Si	Sialic acid-mimic penta-peptide	H1N1, H3N2	400 PFU/mL	[45]
CA	SPCE/PVC membrane	Anti HA Ab/MB/GO/SPCE/PVC membrane	HA protein	8.3 pM/mL	[46]
CA	Au electrode/Si	Antibody/RGO/CA/Au	H1N1	0.5 PFU/mL	[47]
EIS	Au electrode/Si	α-2,6-sialyltransferase enzyme, α-2,3-sialyltransferase enzyme	H1N1	0.05 µg /mL or 2×10^{5} virus/µL	[48]
Amperometric	GCE and SPCE/PVC membrane	Sialic acid derivative	H1N1, H3N2	100 PFU/mL	[49]
DPV	CPE/Paper	Anti-influenza A antibody	H1N1	113 PFU/mL	[47]
EIS	shellac-derived TrGO/ITO/glass	Anti-influenza A antibody	H1N1	26.04 PFU/mL (PBS) 33.11 PFU/mL (Saliva)	Present study

To assess the reproducibility of the devices, five different sensors were tested in 1× PBS at a virus concentration of 1000 PFU/mL (Figure 6a); a significantly small relative standard deviation (2.06 %) was observed, demonstrating high reproducibility. The specificity of the proposed sensors was

evaluated using adenovirus, influenza B virus, and MS2 bacteriophage, whose concentrations were all 1000 PFU/mL in 1× PBS (Figure 6b). The resistance of the sensors increased to 617.94 Ω after the H1N1 virus immobilization while the resistances exhibited negligible changes relative to the EA/Ab/TrGO/ITO/glass electrodes for the other viruses, confirming the specificity for the influenza virus H1N1. Figure 6c shows the stability of the sensors, evaluated at a virus concentration of 1000 PFU/mL in 1× PBS; following a first measurement of the R_{ct} values, the sensors were stored at 4 °C for two weeks, after which approximately 90% of the initial values were retained. This high stability and reproducibility, compared to those achieved via other fabrication methods [47, 50-52], can be ascribed to the high adhesion of TrGO due to the presence of phenolic OH [28].

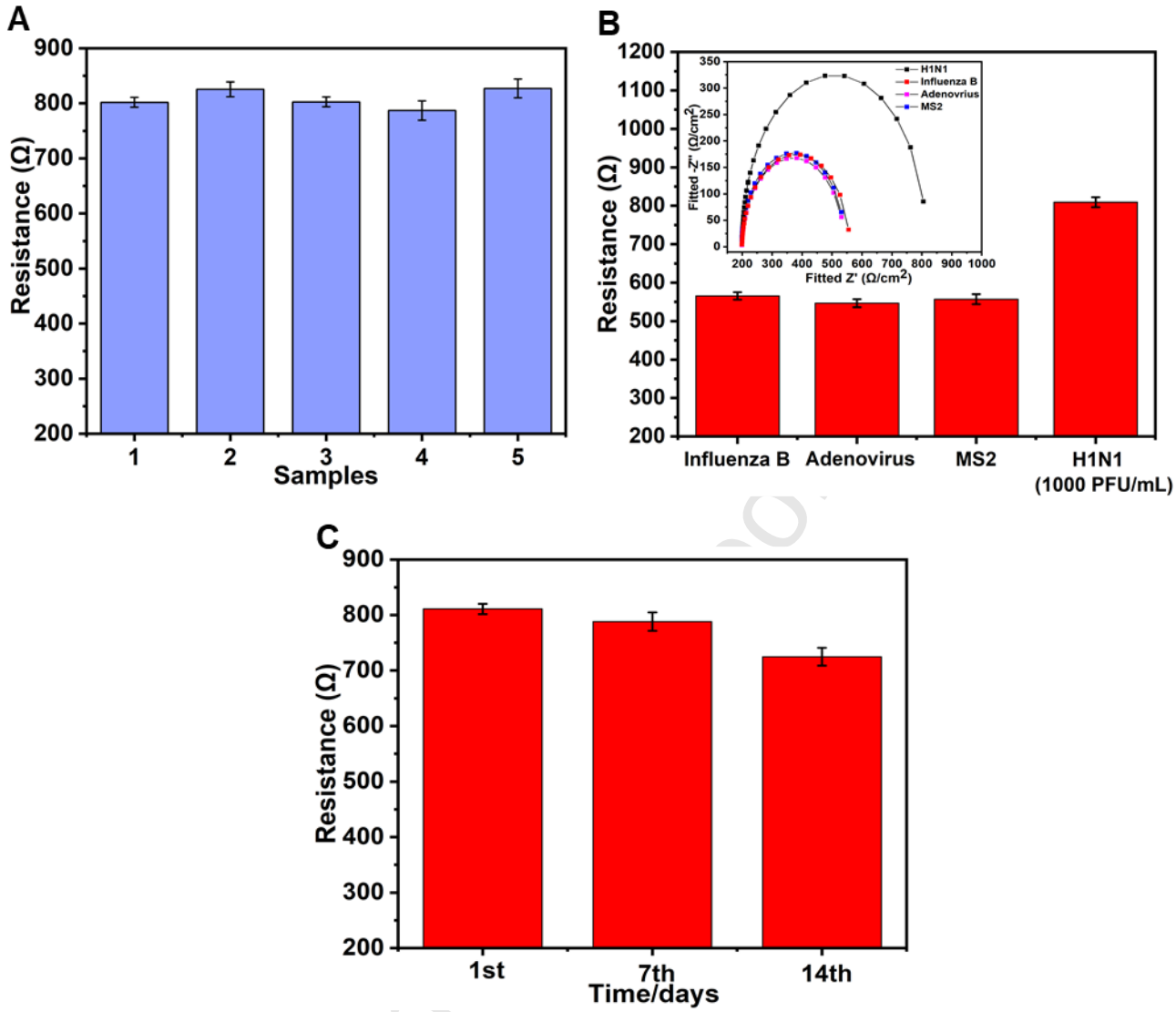

Figure 6. Reproducibility, selectivity, and stability analysis of electrochemical biosensor| (a) Reproducibility of the immunosensors evaluated using an H1N1 virus concentration of 1000 plaque-forming units (PFU)/mL and five different electrodes. (b) The selectivity of the immunosensors evaluated against influenza B virus, adenovirus, and MS2 bacteriophages; the inset shows the respective Nyquist plots. (c) Stability of the immunosensors for two weeks. The error bars represent the standard deviations based on four independent measurements.

4. Conclusion

In conclusion, we have presented the low-cost synthesis of TrGO films from shellac using thermal decomposition technique and their use for fabricating label-free electrochemical biosensors to quantitatively detect the influenza virus H1N1. The TrGO flakes were easily synthesized from Shellac and showed excellent structural, electrical, and electrochemical properties. These cost-effective TrGO-based sensors also showed high stability and reproducibility. The limits of detection for the target virus in PBS and saliva samples were estimated to be 26 and 33 PFU/mL, respectively. The proposed shellac-derived TrGO is expected to be used to fabricate a wide variety of immunosensors and has the potential for large-scale production of functionalized graphene.

Acknowledgments

This research was supported by the National Research Foundation of Korea (NRF) grant funded by the Korea government (MSIT) (No. 2019R1H1A2039725), and also supported by the 2018 Research Fund (1.180015.01) of UNIST.

Appendix A. Supplementary Data

Supplementary data to this article can be found online.

Figure Captions:

Figure 1. Characteristics of the thermally-decomposed reduced graphene oxide (TrGO) films synthesized from shellac: (a) X-ray diffraction spectra revealing its crystalline nature; (b) high-resolution C 1s X-ray photoelectron spectra; (c) Raman spectra showing the G and D bands along with (inset) the 2D band; (d) Fourier transform infrared (FTIR) spectra showing its highly graphitic nature.

Figure 2. Microcrystalline structural analysis of thermally reduced graphene oxide| (a) Transmission electron microscope images of few-layered thermally-decomposed reduced graphene oxide (TrGO) obtained from shellac. (b) High-resolution TEM (HRTEM) image taken at the edge of the TrGO flake showing few-layered features. (c) Zoomed-in image of HRTEM (square box) showing the crystalline nature of TrGO. (d) Selective area diffraction pattern of TrGO showing the hexagonal structure of TrGO.

Figure 3. Electrochemical properties of thermally reduced graphene oxide| (a) Cyclic voltammograms (CVs) at a scan rate of 50 mV/s, and (b) Nyquist plots of indium tin oxide (ITO)/glass, graphene oxide (GO)/ITO/glass, hydrazine-treated reduced GO (rGO)/ITO/glass, and thermally-decomposed rGO (TrGO)/ITO/glass electrodes in the presence of 1× phosphate-buffered saline (PBS) solution containing 5 mM $[Fe(CN)_6]^{3-/4-}$ and 0.5 M KCl as redox mediator. (c) CVs and (d) EIS (Nyquist plots) of ITO/glass, TrGO/ITO/glass, antibody (Ab)/TrGO/ITO/glass, and ethanolamine (EA)/Ab/TrGO/ITO/glass in the presence of 1× PBS containing 5 mM $[Fe(CN)_6]^{3-/4-}$ and 0.5 M KCl as redox mediator.

Figure 4. Optimization of TrGO and H1N1 antibody concentrations| (a) Optimization of TrGO concentration (1 µg/mL to 500 µg/mL) on ITO/glass electrodes. **(b)** The changes in current with H1N1 antibody concentrations (1 µg/mL to 50 µg/mL) on the TrGO/ITO/glass electrodes (the inset showing DPV response) in the presence of 1× PBS containing 5 mM $[Fe\ (CN)_6]^{3-/4-}$ and 0.5 M KCl as redox mediator. The error bars represent the standard deviations based on four independent measurements.

Figure 5. Linear response curve of electrochemical biosensor| Calibration curves based on electrochemical impedance spectra for the quantitative detection of H1N1 virus concentrations between 0 and 10000 (10, 100, 500 1000, 2500, 5000, and 10000) plaque-forming units (PFU)/mL in (a) phosphate-buffered saline (PBS, pH 7.4, 1×) and (b) spiked saliva samples in PBS. The insets show the Nyquist plots in the presence of 1× PBS containing 5 mM $[Fe(CN)_6]^{3-/4-}$ and 0.5 M KCl as a redox mediator. The error bars represent the standard deviations based on four independent measurements.

Figure 6. Reproducibility, selectivity, and stability analysis of electrochemical biosensor| (a) Reproducibility of the immunosensors evaluated using an H1N1 virus concentration of 1000 plaque-forming units (PFU)/mL and five different electrodes. (b) The selectivity of the immunosensors evaluated against influenza B virus, adenovirus, and MS2 bacteriophages; the inset shows the respective Nyquist plots. (c) Stability of the immunosensors for two weeks. The error bars represent the standard deviations based on four independent measurements.

References

[1] X. Cui, A. Das, A.N. Dhawane, J. Sweeney, X. Zhang, V. Chivukula, S.S. Iyer, Chem Sci, 8 (2017) 3628-3634.

[2] K. Kiilerich-Pedersen, J. Dapra, S. Cherre, N. Rozlosnik, Biosens Bioelectron, 49 (2013) 374-379.

[3] M. Heron, National Vital Statistics Reports, 67 (2018) 77.

[4] J.K. Taubenberger, J.C. Kash, Cell Host Microbe, 7 (2010) 440-451.

[5] N. Nikitin, E. Petrova, E. Trifonova, O. Karpova, Adv Virol, 2014 (2014) 859090.

[6] J. Bhardwaj, N. Chaudhary, H. Kim, J. Jang, Anal Chim Acta, 1064 (2019) 94-103.

[7] D. Li, J. Wang, R. Wang, Y. Li, D. Abi-Ghanem, L. Berghman, B. Hargis, H. Lu, Biosens Bioelectron, 26 (2011) 4146-4154.

[8] T.M. Peduru Hewa, G.A. Tannock, D.E. Mainwaring, S. Harrison, J.V. Fecondo, J Virol Methods, 162 (2009) 14-21.

[9] L.R. Farris, N. Wu, W. Wang, L.J. Clarizia, X. Wang, M.J. McDonald, Anal Bioanal Chem, 396 (2010) 667-674.

[10] C. Qi, X.S. Tian, S. Chen, J.H. Yan, Z. Cao, K.G. Tian, G.F. Gao, G. Jin, Biosens Bioelectron, 25 (2010) 1530-1534.

[11] T.J. Park, S.J. Lee, D.K. Kim, N.S. Heo, J.Y. Park, S.Y. Lee, Talanta, 89 (2012) 246-252.

[12] Q. He, S. Velumani, Q. Du, C.W. Lim, F.K. Ng, R. Donis, J. Kwang, Clin Vaccine Immunol, 14 (2007) 617-623.

[13] M. Lin, P. Song, G. Zhou, X. Zuo, A. Aldalbahi, X. Lou, J. Shi, C. Fan, Nat Protoc, 11 (2016) 1244-1263.

[14] D. Nidzworski, K. Siuzdak, P. Niedzialkowski, R. Bogdanowicz, M. Sobaszek, J. Ryl, P. Weiher, M. Sawczak, E. Wnuk, W.A. Goddard, 3rd, A. Jaramillo-Botero, T. Ossowski, Sci Rep, 7 (2017) 15707.

[15] D. Nidzworski, P. Pranszke, M. Grudniewska, E. Krol, B. Gromadzka, Biosens Bioelectron, 59 (2014) 239-242.

[16] E.D. de Asis, Jr., J. Leung, S. Wood, C.V. Nguyen, Nanotechnology, 21 (2010) 125101.

[17] W.A. El-Said, T.H. Kim, H. Kim, J.W. Choi, Nanotechnology, 21 (2010) 455501.

[18] S. Marin, A. Merkoci, Nanotechnology, 20 (2009) 055101.

[19] Y. Liu, X. Dong, P. Chen, Chem Soc Rev, 41 (2012) 2283-2307.

[20] H.G.S. Qiyuan He, Zongyou Yin, Shixin Wu, Hai Li, Freddy Boey, Wei Huang, Peng Chen, and Hua Zhang, ACS Nano, 4 (2010) 8.

[21] Q.H. Herry Gunadi Sudibya, Hua Zhang, and Peng Chen, ACS Nano, 5 (2011) 5.

[22] Z. Yin, Q. He, X. Huang, J. Zhang, S. Wu, P. Chen, G. Lu, P. Chen, Q. Zhang, Q. Yan, H. Zhang, Nanoscale, 4 (2012) 293-297.

[23] Y. Li, K. Sheng, W. Yuan, G. Shi, Chem Commun (Camb), 49 (2013) 291-293.

[24] G. Eda, M. Chhowalla, Adv Mater, 22 (2010) 2392-2415.

[25] H. Feng, R. Cheng, X. Zhao, X. Duan, J. Li, Nat Commun, 4 (2013) 1539.

[26] S.W. Baek, J.W. Ha, M. Yoon, D.H. Hwang, J. Lee, ACS Appl Mater Interfaces, 10 (2018) 18948-18955.

[27] S.-J. Byun, H. Lim, G.-Y. Shin, T.-H. Han, S.H. Oh, J.-H. Ahn, H.C. Choi, T.-W. Lee, The Journal of Physical Chemistry Letters, 2 (2011) 493-497.

[28] Y.N. Singhbabu, S.K. Choudhary, N. Shukla, S. Das, R.K. Sahu, Nanoscale, 7 (2015) 6510-6519.

[29] Y.N. Singhbabu, B. Sivakumar, S.K. Choudhary, S. Das, R.K. Sahu, Surface and Coatings Technology, 349 (2018) 119-132.

[30] S. Panda, T.K. Rout, A.D. Prusty, P.M. Ajayan, S. Nayak, Adv Mater, 30 (2018).

[31] L. Stobinski, B. Lesiak, A. Malolepszy, M. Mazurkiewicz, B. Mierzwa, J. Zemek, P. Jiricek, I. Bieloshapka, Journal of Electron Spectroscopy and Related Phenomena, 195 (2014) 145-154.

[32] R. Singh, S. Hong, J. Jang, Sci Rep, 7 (2017) 42771.

[33] J. Lin, Z. Peng, Y. Liu, F. Ruiz-Zepeda, R. Ye, E.L. Samuel, M.J. Yacaman, B.I. Yakobson, J.M. Tour, Nat Commun, 5 (2014) 5714.

[34] O. Akhavan, Carbon, 48 (2010) 509-519.

[35] V.B. Mohan, R. Brown, K. Jayaraman, D. Bhattacharyya, Materials Science and Engineering: B, 193 (2015) 49-60.

[36] L.M. Malard, M.A. Pimenta, G. Dresselhaus, M.S. Dresselhaus, Physics Reports, 473 (2009) 51-87.

[37] D. López-Díaz, M. López Holgado, J.L. García-Fierro, M.M. Velázquez, The Journal of Physical Chemistry C, 121 (2017) 20489-20497.

[38] D. Yang, A. Velamakanni, G. Bozoklu, S. Park, M. Stoller, R.D. Piner, S. Stankovich, I. Jung, D.A. Field, C.A. Ventrice, R.S. Ruoff, Carbon, 47 (2009) 145-152.

[39] K. Li, H. Zheng, H. Zhang, W.-w. Zhang, K. Li, J. Xu, RSC Advances, 6 (2016) 55618-55625.

[40] S. Brajnicov, A. Bercea, V. Marascu, A. Matei, B. Mitu, Coatings, 8 (2018).

[41] C. Wang, J. Ni, J. Zhou, J. Wen, X. Lü, RSC Advances, 3 (2013).

[42] D.H. Seo, S. Pineda, J. Fang, Y. Gozukara, S. Yick, A. Bendavid, S.K. Lam, A.T. Murdock, A.B. Murphy, Z.J. Han, K.K. Ostrikov, Nat Commun, 8 (2017) 14217.

[43] S. Yezli, J.A. Otter, Food and Environmental Virology, (2011).

[44] R. Wang, Y. Wang, K. Lassiter, Y. Li, B. Hargis, S. Tung, L. Berghman, W. Bottje, Talanta, 79 (2009) 159-164.

[45] T. Matsubara, M. Ujie, T. Yamamoto, M. Akahori, Y. Einaga, T. Sato, Proc Natl Acad Sci U S A, 113 (2016) 8981-8984.

[46] M. Veerapandian, R. Hunter, S. Neethirajan, Talanta, 155 (2016) 250-257.

[47] S. Devarakonda, R. Singh, J. Bhardwaj, J. Jang, Sensors (Basel), 17 (2017).

[48] B. Wicklein, M.Á.M. del Burgo, M. Yuste, E. Carregal-Romero, A. Llobera, M. Darder, P. Aranda, J. Ortín, G. del Real, C. Fernández-Sánchez, E. Ruiz-Hitzky, Advanced Functional Materials, 23 (2013) 254-262.

[49] X. Zhang, A.N. Dhawane, J. Sweeney, Y. He, M. Vasireddi, S.S. Iyer, Angew Chem Int Ed Engl, 54 (2015) 5929-5932.

[50] A. Sharma, J. Jang, Sci Rep, 9 (2019) 5970.

[51] J. Bhardwaj, A. Sharma, J. Jang, Biosens Bioelectron, 126 (2019) 36-43.

[52] A. Sharma, C.H. Han, J. Jang, Biosens Bioelectron, 82 (2016) 78-84.

Graphical abstract

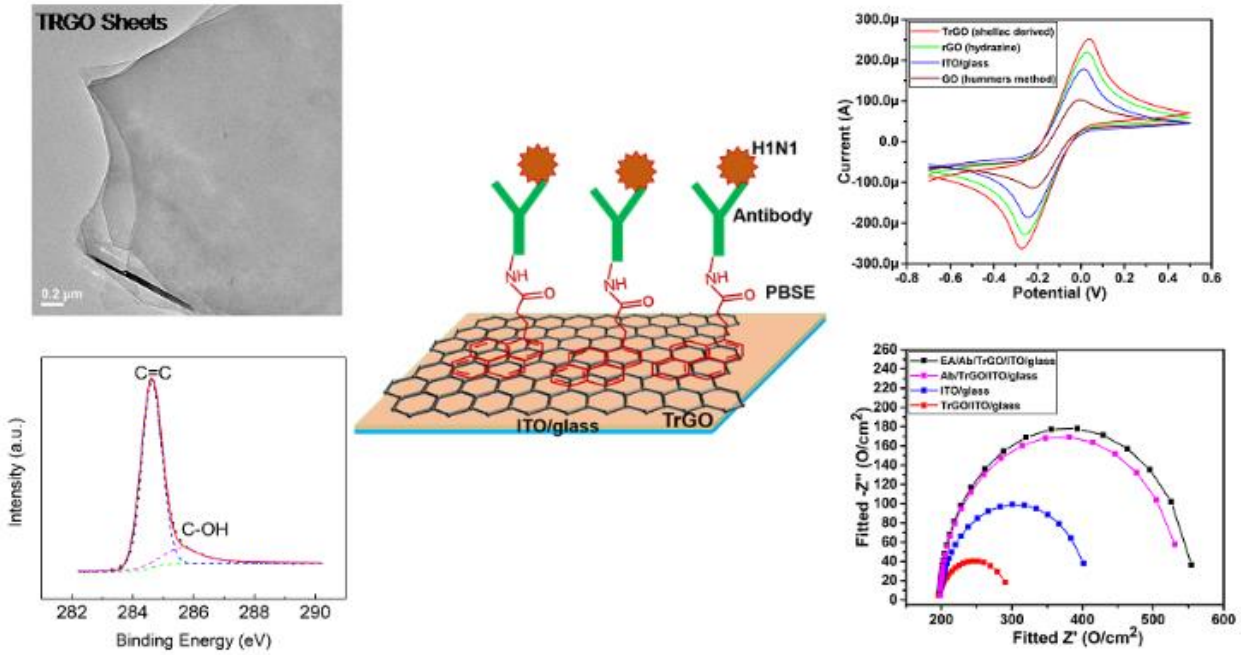

Highlights

1. Green approach was used as a carbon precursor to synthesize TrGO films.

2. These films display low sheet resistance (200 Ω/□) with extremely high carbon content (97%).

3. Electrochemical biosensing platform was made for the detection of H1N1 virus.

4. These sensors display high stability, selectivity and reproducibility.

5. The LOD was obtained to be 26 and 33 plaque-forming units, respectively, in PBS and diluted saliva.